Available online at www.sciencedirect.com
SCIENCE DIRECT®
Journal of Power Sources 134 (2004) 170–180
JOURNAL OF POWER SOURCES
www.elsevier.com/locate/jpowsour

Pt–Ru_{adatom} nanoparticles as anode catalysts for direct methanol fuel cells

Dianxue Cao, Steven H. Bergens*

Department of Chemistry, University of Alberta, Edmonton, Alberta, Canada T6G 2G2

Received 4 March 2004; accepted 22 March 2004

Available online 10 June 2004

Abstract

A series of prototype direct methanol fuel cells (DMFCs) were constructed and operated under identical procedures and conditions except for the surface compositions of the anode electrocatalysts. The cathode electrocatalyst was Pt black (loading 2 mg/cm^2, specific surface area: ca. 27 m^2/g), the electrolyte membrane was Nafion^{TM} 117, and the anode electrocatalysts were a series of Pt–Ru adatom (Pt–Ru_{ad}) nanoparticles (loading 2 mg/cm^2, specific surface area: ca. 27 m^2/g) prepared by a direct surface reductive deposition of Ru_{ad} onto Pt black. The optimum surface coverage of Pt by Ru_{ad} was ca. 33% for DMFCs operating at 60 °C. The optimum ranged from ca. 30 to 60% at 90 °C. A DMFC using Pt–Ru_{ad} nanoparticles supported on carbon (Vulcan XC-72^{TM}) as anode electrocatalyst was operated for 20 days at 8 h each day without loss of activity. These results, combined with those from an in situ cyclic voltammetry study, indicate that no significant Ru_{ad} dissolution and/or redistribution occurred during fabrication and operation of the prototype DMFCs.

Keywords: Platinum; Ruthenium; Adatom; Direct methanol fuel cell; Anode electrocatalyst

1. Introduction

We report a series of direct methanol fuel cells (DMFCs) using Pt–Ru adatom nanoparticles (Pt–Ru_{ad}) as anode electrocatalysts. The development of highly effective, and economical methanol electrooxidation catalysts is a topic of intense research efforts [1]. Pt-based binary [2], ternary [3] and quaternary [4] catalysts are active toward methanol electrooxidation, and they are stable in acidic media. First reported during the mid-1960s [5–7], Pt–Ru nanoparticle systems remain as the most studied and as the state-of-the-art methanol electrooxidation catalyst in the anodes of prototype DMFCs [8,9]. Preparation of Pt–Ru electrocatalysts by deposition of submonolayer amounts of Ru_{ad} onto Pt substrates provides a level of control over real surface area (number of active sites) and surface composition (ratio of moles surface Pt atoms ($Pt_{surface}$) to moles Ru_{ad} deposited) that is difficult to achieve using other catalyst preparations. The methods used to prepare Pt–Ru_{ad} catalysts include electrochemical deposition of Ru_{ad} onto single crystal Pt (Pt($h\,k\,l$)) [10–18] or polycrystalline Pt [19–22], evaporative deposition of Ru atoms onto Pt($h\,k\,l$) [11,23–28], and chemical vapor deposition onto Pt($h\,k\,l$) [29,30].

Several non-electrochemical depositions of Ru_{ad} onto Pt substrates carried out in solution (thereby being well-suited for preparation of nanoparticles) have been reported. The most studied is the often-termed spontaneous depositions developed by Wieckowski and coworkers [10–13,31–41]. This deposition involves the adsorption of Ru species from aged perchloric acid solutions of $RuCl_3$ onto Pt, followed by electrochemical reduction of the Ru deposits to generate strongly adsorbed, mainly metallic Ru_{ad}. Studies of this deposition using Pt($h\,k\,l$) as substrate show that the rate of Ru deposition [32,38], the degree of preference for two-dimensional over three-dimensional Ru_{ad} island growth [36,39–41], as well as the optimum surface composition and activity for methanol electrooxidation are surface structure dependant [10–12,32]. This process is also a rare example of an adatom deposition used to prepare Pt–Ru_{ad} nanoparticles [35]. Pt–Ru_{ad} nanoparticles prepared this way have been studied by EC-NMR spectroscopy [29,30,36,42], by voltammetry, by CO stripping voltammetry, and as catalysts for the electrooxidation of methanol and formic acid [29,30,35,36]. A spontaneous-type deposition developed by Vielstich and coworkers involves reaction of aqueous $RuCl_3$ with clean Pt [24,25]. This deposition is proposed to proceed via prior ad-

* Corresponding author. Tel.: +1-780-492-9703; fax: +1-780-492-8231.
E-mail address: steve.bergens@ualberta.ca (S.H. Bergens).

0378-7753/$ – see front matter © 2004 Elsevier B.V. All rights reserved.
doi:10.1016/j.jpowsour.2004.03.053

sorption of chloride onto the Pt surface with dissolved Ru^{3+} ions acting as counter ions for the adsorbed chloride. Electrochemical reduction was then used to generate Pt–Ru_{ad} and to desorb the chloride ions from the surface. Both of these depositions are self-limiting: they cease after a specific submonolayer amount of Ru_{ad} precursor is deposited onto the Pt surface and they can be repeated to obtain incrementally higher amounts of Ru_{ad} than those obtained from single deposition.

A non-electrochemical deposition that directly generates Ru_{ad} in reduced form involves hydrogenation of $Ru(COD)(\eta^3\text{-}C_3H_5)_2$ (COD is 1,5-cyclooctadiene) over Pt in hexane under mild conditions (−40 to −15 °C, 1 atm H_2) to generate Pt–Ru_{ad}, cyclooctane, and propane [43,44]. A related deposition uses $Ru_4H_4(CO)_{12}$ to deposit Ru_{ad} and CO onto Pt nanoparticles under H_2 in hexanes [45]. This deposition is self-limiting: further deposition beyond ca. 0.1 surface equivalents of Ru_{ad} is poisoned by adsorbed CO. Ru_{ad} have also been deposited by adsorbing the ruthenium cluster $[Ru_3(CO)_9(MeCN)_3]$ onto Pt surfaces followed by decomposition of the adsorbed species under hydrogen [46,47].

A self-limiting, directly reductive deposition carried out in water using $RuCl_3$ as Ru_{ad} source was developed by Janssen and Moolhuysen in 1975 [48,49]. A related version was later studied by Szabó et al. [50,51]. Janssen and coworkers electrochemically cleaned the Pt substrate in aqueous H_2SO_4, saturated the Pt surface with adsorbed hydrogen at 0.05 V versus RHE, and then transferred the surface to an aqueous solution of $RuCl_3$. The hydrogen adsorbed on the Pt surface reduced an undetermined amount of $RuCl_3$(aq) to deposit Ru_{ad} onto the surface. Barbier and coworkers prepared a series of M–M'_{ad} catalysts for non-electrochemical reactions (e.g. Pt–Au_{ad}, Pt–Cu_{ad}, Pd–Pt_{ad}, Pt–Re_{ad}, and Ru–Cu_{ad}) using a similar methodology [52–60].

We recently reported a non-electrochemical, aqueous method to clean the surface of Pt black, to saturate its surface with hydrogen, and to carry out repeated reductive depositions of Ru_{ad} using aqueous $RuCl_3{\cdot}xH_2O$ ($x = 1$–3) as the adatom source. Eq. (1) shows the idealized stoichiometry of the reaction [61]. We found that the reaction

$$3Pt_{surf}\text{–}H + RuCl_3(aq) \rightarrow (Pt_{surf})_3\text{–}Ru_{ad} + 3Cl^- + 3H^+ \quad (1)$$

deposited ca. 0.18 surface equivalents of Ru_{ad} (the ratio of Ru_{ad} deposited to Pt_{surf} originally on the substrate) rather than the theoretical maximum of 0.33 equivalents. The resulting Pt–Ru_{ad} nanoparticles were studied using cyclic voltammetry, CO-stripping voltammetry, and as catalysts for electrooxidation of methanol in three-electrode experiments. The optimum Ru surface coverage for electrooxidation of methanol over these nanoparticles in three-electrode experiments was ca. 0.33 (0.4 V versus RHE, 60 °C, $[H_2SO_4] = [MeOH] = 1.0$ M, we designate this catalyst as Pt–Ru_{ad}-0.33). Our results agreed with those of Wieckowski and coworkers [35,36]. Nanoparticle Pt–Ru_{ad} catalysts, prepared using either the reductive deposition method reported by us, or using the spontaneous deposition technique developed by Wieckowski and coworkers, are almost twice as active (current per active site) as the state-of-the-art commercial Pt–Ru alloy catalysts (Johnson Matthey HiSPEC-6000™). We also reported initial data from a series of prototype DMFCs using the Pt–Ru_{ad} nanoparticles as anode catalyst and found that ca. 0.33 was the optimum Ru surface coverage for fuel cells operating on methanol at 60 °C. Reports of adatom systems as anode catalysts in actual prototype DMFCs are rare [45], and whether such adatom catalysts can survive incorporation and operation in a fuel cell has been questioned in the literature [1,62,63]. For example, Wasmus and Kuver [1] state that neither chemisorbed nor electrosorbed foreign metals on Pt are a practical way to make fuel cell catalysts because variations in cell voltages during fuel cell operation may lead to desorption of the foreign metal into the electrolyte. Further, surface segregation of Pt–Ru systems has been observed under certain conditions. For example, Ross and coworkers [62] observed a strong surface enrichment in Pt for Pt–Ru alloys annealed at 800 °C in UHV. Arico et al. [64] also recently reported that Pt enrichment occurs in practical nanoparticle Pt–Ru alloy catalysts, particularly those with low bulk Ru content alloys. These studies suggest that surface segregation of Pt–Ru_{ad} systems may occur during the fabrication and operation of DMFCs, and that segregation may limit the lifetimes and activities of Pt–Ru_{ad} nanoparticle catalysts.

We now report a detailed analysis that studied the electrocatalytic activity and stability of Pt–Ru_{ad} nanoparticles as anode catalysts in a series of prototype DMFCs under various operating conditions.

2. Experimental

2.1. Preparation of Pt–Ru_{ad} catalysts

The nanoparticle unsupported and carbon-supported Pt–Ru_{ad} catalysts were prepared by the surface reductive deposition method described in our previous paper [61]. In brief, platinum substrates (Pt black, Johnson Matthey HiSPEC™-1000, 27 m^2/g, Pt/C with 20 wt.% Pt, 112 m^2/g, and 40 wt.% Pt, 72 m^2/g from E-TEK) were first cleaned with 3% H_2O_2 (ACP Chemicals Inc., Reagent ACS, 30%) and then maintained in the remaining water in the reactor. The reactor was flushed with argon (Praxair, pre-purified) to remove any oxygen, then flushed with hydrogen (generated by a hydrogen generator, Peak™ Scientific) to reduce the platinum oxide surface to form adsorbed H on Pt_{surf}. The system was then flushed with argon to eliminate the excess H_2. An argon-purged, freshly made 0.05 M $RuCl_3$ (AITHACH Chemical Corp.) aqueous solution was introduced into the reactor under argon protection. The solution

Table 1
Pt–Ru_{ad} catalysts prepared by surface reductive deposition of Ru onto nanoparticle Pt and Pt/C

	Pt substrates								
	Unsupported Pt–Ru_{ad} (Pt black)					Carbon-supported Pt–Ru_{ad} (Pt/C)			
						20 wt.% Pt	20 wt.% Pt	20 wt.% Pt	40 wt.% Pt
Number of depositions	1	2	3	5	7	1	2	3	2
Surface equivalent Ru (φ)	0.18	0.38	0.57	0.85	1.31	0.58	0.74	0.85	/
Estimated Ru surface coverage (θ)	0.18	0.33	0.45	0.63	0.75	NA	NA	NA	NA

was stirred under argon for 1 h to complete the deposition. The Pt–Ru_{ad} nanoparticles were separated from the liquid by vacuum filtration in air, then thoroughly washed with pure water, and dried under vacuum for 24 h. The deposition was repeated as many times as needed to obtain Pt–Ru_{ad} with high Ru surface coverage.

Also as described in detail in our previous paper [61], in order to measure the amount of Ru_{ad} deposited on the Pt, Ru_{ad} was first oxidatively stripped from the surface by stirring the Pt–Ru_{ad} or the Pt–Ru_{ad}/C in a saturated solution of $K_2S_2O_8$ (Fisher Scientific, Certified Reagent) in 4.0 M KOH (BDH Inc., ACS) for 1 h [65]. The resulting aqueous solutions of Ru ions were then analyzed using inductively coupled plasma-atomic emission spectrometry (ICP-AES; Perkin-Elmer Optima) to give the amount of Ru deposited [43,61]. The surface equivalents of Ru were then calculated using the amount of Ru measured and the real surface area of the Pt substrate (1.31×10^{15} atom/cm^2 [66]). The results were given in Table 1. The Ru surface coverages (the fraction of Ru_{ad} among the surface atoms on the catalyst) were estimated for unsupported Pt–Ru_{ad} (Table 1) as described in our previous paper [61]. This estimation is not applicable to carbon supported Pt–Ru_{ad} (see text). The catalyst samples in this study were designated as Pt–Ru_{ad}-θ (unsupported) and Pt–Ru_{ad}/C-φ (supported), θ is the estimated Ru surface coverage, φ is the surface equivalents of Ru.

2.2. Fabrication of membrane electrode assemblies

Membrane electrode assemblies (MEAs) of geometrical area 5 cm^2 were prepared as described in our previous publication [61]. Briefly, the fabrication procedure consists of three steps: preparation of catalyst inks, painting, and hot-pressing. The unsupported catalyst inks were prepared by suspending the catalyst in water and sonicated for 30 min to thoroughly wet and disperse the catalyst. Enough 5% Nafion^{TM} solution (ElectroChem Inc.) was added to the mixture to give a dry ink composition of 80 wt.% catalyst with 20 wt.% Nafion^{TM} ionomer. The mixtures were sonicated for another 2 h at room temperature to obtain uniformly dispersed inks. The carbon-supported catalyst inks were prepared by suspending the catalyst in 5% Nafion^{TM} solution diluted with 2-propanol (e.g. 200 mg Nafion^{TM} solution in 65 mg 2-propanol) to give a dry ink composition of 70 wt.% catalyst with 30 wt.% Nafion^{TM} ionomer. The mixtures were stirred and sonicated alternately (1 h stirring, 1 h sonicating) for a total of 6 h. The catalyst inks were painted onto 5 cm^2 Teflon^{TM} decals at around 70 °C, and then baked in an oven at 135 °C for 5 min to cure the catalyst/Nafion^{TM} composite. Nafion^{TM}-117 membranes (Alfa Aesar) were cleaned and converted into the acid form by boiling in 3% H_2O_2 for 1 h, in 0.5 M H_2SO_4 (Alfa Aesar, 99.9999%) for 2 h, and in ultra-pure water for 2 h with the water being changed every 30 min. The cleaned membranes were stored in ultra-pure water, and dried on a vacuum table at 60 °C for 45 min immediately before use. The catalyst layers were transferred from the Teflon^{TM} decals to the Nafion^{TM} membranes by hot-pressing at 125–127 °C, 1450–1550 psig for ca. 2.5 min.

2.3. Operation of direct methanol fuel cells

The MEAs were mounted into commercial fuel cell hardware (ElectroChem Inc., FC05-01SP). The current collectors were made of low-porosity, high-purity graphite blocks with serpentine flow fields. The cell was held between two gold-plated copper contact plates using a set of retaining bolts positioned around the periphery of the cell. Electrical heaters were placed behind each of the copper plates. Separate voltage connectors and thermocouple wells were in each cell block to provide accurate measurement and temperature control. Teflon^{TM}-treated carbon paper (ElectroChem Inc., 30 wt.% polytetrafluoroethylene (PTFE)) was used as backing layers to allow for even distribution of reactants. PTFE gaskets were inserted to prevent the cell from leaking. The fuel cells were operated by pumping 1.0 M aqueous methanol (Sigma-Aldrich, ACS HPLC grade, 99.93%) through the anode compartment at 4.0 mL/min, with zero back pressure, from a reservoir at ambient temperature, and by flowing dry oxygen (Praxair) through the cathode compartment at 400 standard cubic centimeters per minute (sccm) at 20 psig back pressure. Pure oxygen was used to maximize the activity of the cathode so that the differences in cell performance would reflect as much as possible the differences in anode catalyst activity. Prior to taking polarization data, the fuel cells were conditioned for 3 days using the following procedure: the DMFC was heated to 60 °C at open circuit with methanol solution circulating through the anode, and with oxygen flowing through the cathode. The cell was then run at 20 mA/cm^2 for 4 h. The

cell temperature was raised to 90 °C, and the cell was operated at 100 mA/cm^2 for another 4 h. The cell was then shut down by turning off the load, heat, methanol and oxygen supply, and left overnight at room temperature. Fresh methanol solution was used the following day. The performance of the DMFCs stabilized after such conditioning. The cell potential–current curves were obtained using an 890 Series computer-controlled fuel cell test load (Scribner Associate Inc.). The reported cell voltages are not IR compensated.

2.4. Cyclic voltammetry

Cyclic voltammetry of the anode and cathode catalyst layers in the assembled, stabilized fuel cells was performed using a Pine Bipotentiostat Model AFCBP1 controlled with Pinechem 2.00 software [67–69]. The cyclic voltammograms were recorded in the fuel cell blocks at ambient temperature, with the working electrode under purified water flowing at 8 mL/min, and the other electrode was used as the counter- and reference electrode by supplying it with humidified H_2 at 100 mL/min at zero back pressure. The temperature of the hydrogen humidifier was 35 °C. The potential was scanned from 0 to 700 mV versus the counter/reference electrode at 10 mV/s.

3. Results and discussion

3.1. Unsupported Pt–Ru$_{ad}$ anode catalysts

Membrane electrode assemblies were fabricated using Pt–Ru$_{ad}$ nanoparticles with various Ru$_{ad}$ surface coverages as the anode catalyst. As much as possible, each prototype DMFC was assembled using the same materials, procedures, and the cells were conditioned the same way. To check for experimental errors that may have occurred during fabrication of the MEAs, two MEAs were fabricated and evaluated for each type of anode catalyst. The results showed that the DMFC polarization data are reproducible. Pt black (Johnson Matthey HiSPEC^{TM}-1000, specific surface area: 27 m^2/g) was used as the cathode catalyst, and Nafion^{TM}-117 was used as the solid electrolyte membrane. The batch of Pt black used for the cathode catalyst was used as substrate to prepare all the Pt–Ru$_{ad}$ anode catalysts via the reductive deposition of Ru$_{ad}$. The catalyst loadings were 2 mg/cm^2 in both the anode and cathode, and the prototype DMFCs were operated at 60 and 90 °C. A pure oxygen feed was used to maximize the activity of the cathode in order for the performance of the DMFCs to reflect differences in Pt–Ru$_{ad}$ anode catalyst activity. As shown in our previous paper [61], the specific surface area of the Pt substrate does not change significantly during this deposition. It is thereby reasonable to expect that the real surface areas of the anodes and cathodes are similar in these series of DMFCs. The utilizations of the Pt cathode catalysts ranged from 80 to 85%, as determined by cyclic voltammetry carried out in the fuel cell (vide infra).

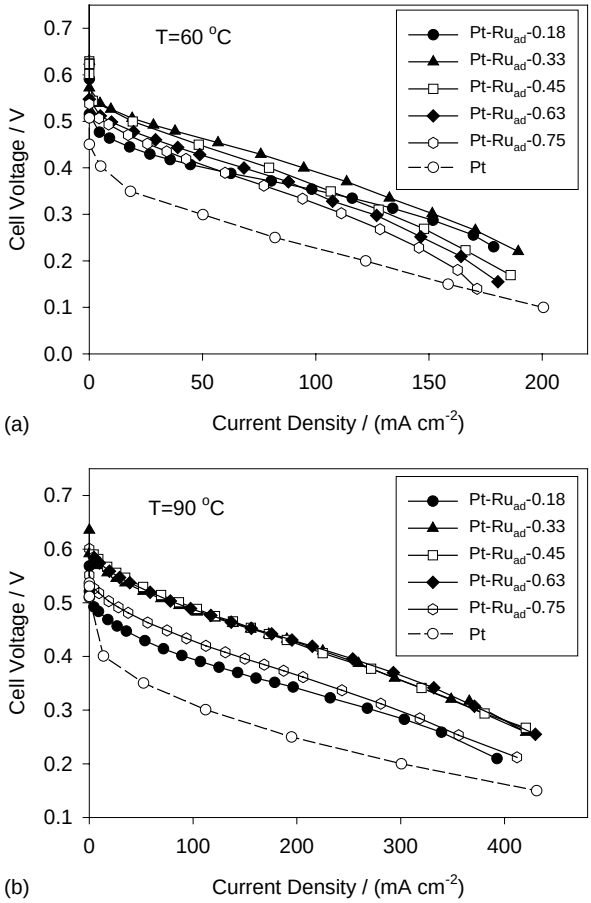

Fig. 1. Polarization curves for a series of DMFCs with Pt–Ru$_{ad}$ anode catalysts of differing surface composition. Anode: 2 mg/cm^2 Pt–Ru$_{ad}$ catalyst, 1.0 M methanol at 4.0 mL/min, and zero back pressure. Cathode: 2 mg/cm^2 Pt-black catalyst, 20 psig dry oxygen at 400 sccm.

The cell polarization curves are shown in Fig. 1. It can be seen that at 60 °C, the best performance was obtained using Pt–Ru$_{ad}$-0.33, followed in decreasing order by Pt–Ru$_{ad}$-0.45, -0.63, -0.75, -0.18, and -0. This activity sequence is consistent with that we obtained in the three-electrode experiments carried out in 1.0 M H_2SO_4 + 1.0 M MeOH at 60 °C [61]. As expected, the DMFC performance improved as the temperature was increased. The order of DMFC performance as a function of surface composition of Pt–Ru$_{ad}$ anode catalyst, however, also changed upon increasing the temperature. At 90 °C, Pt–Ru$_{ad}$-0.33, -0.45, and -0.63 had nearly the same, highest cell performance. This result supports those observations on the dependence of the optimum surface composition of Pt–Ru catalysts on temperature reported in the literature [70,71]. Specifically, the optimum surface composition of shiny, flat Pt–Ru alloys shifts from low to high Ru coverage with increases in temperature. We thereby propose that for a PEM–DMFC operating over a wide temperature range, use of an anode catalyst composed of a mixture of

Pt–Ru catalysts with surface compositions ranging from ca. 10–50% Ru would benefit the overall cell performance versus temperature behavior of the cell. The optimum Ru surface coverage for the DMFCs operating at 90 °C was ca. 50%. Arico et al. [64] studied the optimum surface composition of unsupported Pt–Ru alloy nanoparticles as anode catalyst in DMFCs operated at 130 °C. They found the optimum surface composition, as determined by XPS, was ca. 40% Ru. Lamy and coworkers [72,73] recently reported a optimum composition of 20% Ru for carbon supported Pt–Ru anode catalyst in a single DMFC, irrespective of the working temperature (from 25 to 110 °C).

As shown by Weickowski and coworkers using spontaneous deposition [35], and shown subsequently by us using direct reductive deposition [61,74], Pt–Ru_{ad} nanoparticles are inherently more active toward methanol electrooxidation in three electrode experiments than the state-of-the-art commercial Pt–Ru nanoparticles (Johnson Matthey HiSPEC-6000^{TM}, 1:1 a/o Pt:Ru, specific surface area: ca. 70 m^2/gm [68,75]). For example, Pt–Ru_{ad}-0.33 is 1.6 times more active than the commercial Pt–Ru at 60 °C and 0.4 V (1.0 M H_2SO_4 + 1.0 M MeOH) in terms of the per surface site activity (see insert in Fig. 2a). In order to compare the performance of the Pt–Ru_{ad} nanoparticles with the commercial Pt–Ru alloy nanoparticles in prototype PEM-DMFCs, a membrane electrode assembly was fabricated using the commercial Pt–Ru black as the anode catalyst. This MEA–DMFC was manufactured, conditioned, and operated using the identical procedure as for Pt–Ru_{ad} anode catalysts. Fig. 2 shows the polarization curves of DMFCs with Pt–Ru_{ad}-0.33 and the commercial Pt–Ru anode catalyst. The currents are normalized to the total surface area of the anode catalyst, which was obtained using the specific surface area of the catalyst and the anode catalyst loadings. It can be seen that in the kinetically controlled (low current) region, the commercial Pt–Ru catalyst is more active than Pt–Ru_{ad}-0.33. This order of activity is contrary to the results obtained using the three-electrode cell (1.0 M H_2SO_4 + 1.0 M MeOH) which show that the commercial Pt–Ru nanoparticles are less active than the Pt–Ru_{ad}-0.33 nanoparticles (insert, Fig. 2a). This inversion of the real activity of commercial Pt–Ru versus Pt–Ru_{ad} observed between PEM–DMFCs and three-electrode cells suggests that the commercial Pt–Ru anode structure is different from the Pt–Ru_{ad} anode structure. Catalyst layer structures determine the methanol, CO_2 mass transport, ionic conductivity, and catalyst utilization [76–82]. In this study, the commercial Pt–Ru anode may have a better structure than the Pt–Ru_{ad} anode. In addition, the commercial catalyst may be activated towards methanol electrooxidation during fabrication of the MEA and conditioning of the DMFC. For example, this catalyst contains metal oxides in the as-received form, and these oxides will affect the wettability of the catalyst by Nafion^{TM}. Further they are to some extent reduced during the conditioning and operation of the DMFC, resulting in catalyst surface reconstruction to a better optimized operating catalyst [68,83]. As indicated by our earlier data [45], and as we examine further in this work (vide infra), Pt–Ru_{ad} nanoparticles do not appear to change significantly during fabrication of the MEA and operation of the fuel cells. As a result, it appears that the higher activity of Pt–Ru_{ad} over the commercial alloy measured in the three-electrode cell was overcome in the PEM–DMFC by the differences in electrode structure and in surface reconstruction of the commercial catalyst. This study demonstrates that a good catalyst for fuel cells must be active after incorporation, conditioning, and it must also settle into a suitable electrode structure.

It should be pointed out that the better performance observed on Pt–Ru_{ad}-0.33 than that measured on the commercial Pt–Ru in the high cell current density (low cell voltage) region does not suggest that Pt–Ru_{ad}-0.33 is more active than commercial Pt–Ru. This is simply because in the high current region, methanol and/or CO_2 mass transport dominates the performance of the cell using the commercial catalyst.

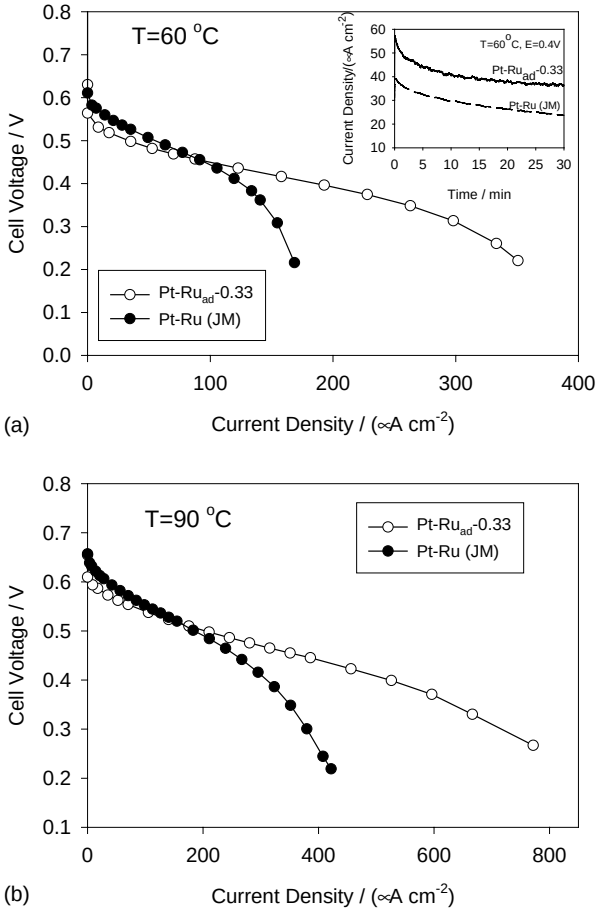

Fig. 2. DMFC polarization curves with currents normalized by the total surface area of the anode catalysts. Anode: 2 mg/cm^2 catalyst, 1.0 M methanol at 4.0 mL/min. Cathode: 2 mg/cm^2 Pt-black catalyst, 20 psig dry oxygen at 400 sccm. The insert is the potentiostatic methanol oxidation current densities normalized by the real surface area of the catalysts. The currents were measured in a three-electrode cell containing 1.0 M MeOH + 1.0 M H_2SO_4.

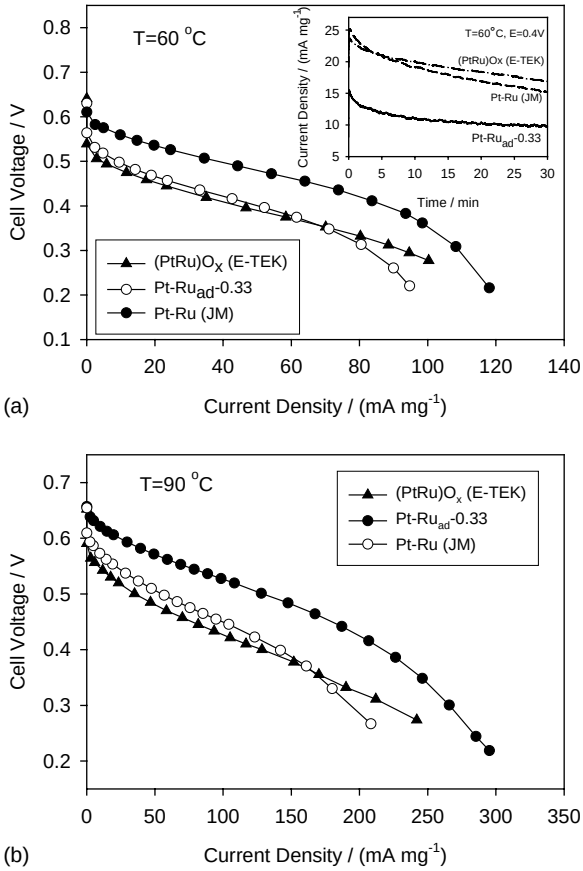

Fig. 3. DMFC polarization curves with currents normalized by the mass of the anode catalyst. Anode: 2 mg/cm^2 catalyst, 1.0 M methanol at 4.0 mL/min. Cathode: 2 mg/cm^2 Pt-black catalyst, 20 psig dry oxygen at 400 sccm. The insert is the potentiostatic methanol oxidation current densities normalized by the mass of the catalysts. The currents were measured in a three-electrode cell containing 1.0 M MeOH + 1.0 M H_2SO_4.

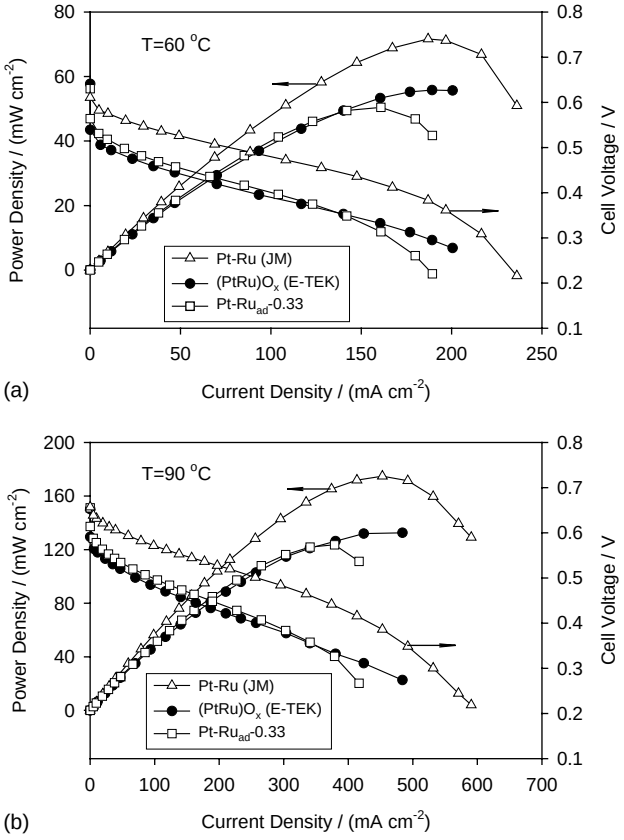

Fig. 4. Power–current and voltage–current curves for DMFCs employing Pt–Ru_{ad}, Pt–Ru from Johnson Matthey and (Pt–Ru)O_x from E-TEK anode catalysts. Anode: 2 mg/cm^2 catalyst, 1.0 M methanol at 4.0 mL/min. Cathode: 2 mg/cm^2 Pt-black catalyst, 20 psig dry oxygen at 400 sccm. Currents are normalized to the geometrical area of the electrodes.

We found (see insert of Fig. 3a) that the mass activities (current per mg catalyst) of Johnson Matthey Pt–Ru alloy and another commercially available catalyst, E-TEK (PtRu)O_x, were nearly the same (ca. 18 mA/mg) in three-electrode experiments (at 60 °C, 0.4 V, 1.0 M H_2SO_4, and 1.0 M MeOH). They were higher than that of Pt–Ru_{ad}-0.33 (ca. 10 mA/mg) because the specific surface areas of these commercial catalysts are quite high. Fig. 3 shows the cell polarization curves with currents normalized to per mg anode catalysts. In contrast with the three-electrode experiments, the mass activity of E-TEK (PtRu)O_x anode catalyst is lower than that of Johnson Matthey Pt–Ru and of Pt–Ru_{ad}-0.33. The poor performance of the E-TEK (PtRu)O_x catalyst in the DMFC likely arises from non-optimal electrode structure or catalyst surface restructuring [78]. The importance of electrode structures and catalyst reconstruction during the fabrication and operation of DMFCs should not be underestimated.

Fig. 4 shows plots of power density versus current density for these DMFCs. Also included in this graph are the cell polarization curves. The peak power output for the Pt–Ru_{ad} cell approaches 125 mW/cm^2 at ca. 400 mA/cm^2 and at 90 °C. This maximum power is about 70% that of the Johnson Matthey Pt–Ru cell (175 mW/cm^2 at ca. 450 mA/cm^2), and it is comparable to that of the E-TEK (PtRu)O_x cell (130 mW/cm^2 at ca. 450 mA/cm^2). The operating temperature has a significant effect on the power output. For example, increasing the operating temperature from 60 to 90 °C increased the peak power density of the Pt–Ru_{ad} cell from 50 to 125 mW/cm^2. In a recent literature example, 400 mW/cm^2 peak power density has been reported for a Nafion^{TM}-112 DMFC (2.2 mg/cm^2 Pt–Ru on anode, 2.2 mg/cm^2 Pt black on cathode) operating at 130 °C on 5 atm oxygen [84]. The anode fuel system must be pressurized to keep the fuel in a liquid state if a cell is operated over 100 °C; however, the design of such a high-temperature liquid feed PEM–DMFC is complex, and was not pursued for this investigation. We point out that electrode structure, flow fields, cell shape, current collectors, and other factors all affect the performance of DMFCs [80,85–87]. Our DMFCs were not optimized for all these factors, they were optimized for consistency.

3.2. Carbon-supported Pt–Ru_{ad} anode catalysts

We prepared a series of carbon-supported Pt–Ru_{ad} catalysts using Pt on Vulcan™ XC-72R (20 wt.% Pt, specific surface area: 112 m^2/g, E-TEK) as substrate by the direct reductive deposition (Table 1). It appears that Ru^{3+} was not only reduced by $Pt_{surface}$–H leading to the formation of Pt–Ru_{ad} nanoparticles, but it was also adsorbed onto the surfaces of the carbon support. This is suggested by the high number of surface equivalents of Ru_{ad} that were obtained after a single deposition onto Pt/C, ca. 0.58. This amount is larger than the maximum (0.33) that could be obtained if the Ru_{ad} was deposited only by reaction with $Pt_{surface}$–H (Eq. (1)), and as discussed in our previous paper [61]. It is likely that the Ru^{3+} adsorbed by the carbon support was reduced by methanol during operation of the DMFC, resulting in a (Pt–Ru_{ad} + Ru)/C catalyst. It is not possible to discriminate between the Ru on Pt surfaces and on carbon surfaces with the data obtained during this study. A TEM analysis will be carried out in the future to address this issue. The surface equivalents of Ru (expressed as a percentage of the number of Ru_{ad} deposited to the number of surface atoms of Pt on the substrate) thereby does not reflect the surface ratio of Ru_{ad} to $Pt_{surface}$ in the Pt–Ru_{ad} phase, but it serves as an indication of the total amount of Ru deposited. MEAs were fabricated using Pt–Ru_{ad}/C as anode catalyst and unsupported Pt black as cathode catalyst. The cathode catalyst loading was maintained at 2 mg/cm^2. The anode catalyst loading was ca. 0.65 mg/cm^2 for Pt–Ru_{ad}/C. Smotkin and coworkers [88] reported that MEAs prepared using Pt–Ru/C (20 wt.% metal loading, 1:1 a/o Pt:Ru) as anode catalyst showed no improvement in cell performance with anode loadings above ca. 0.5 mg/cm^2. We found that it is difficult to transfer (Pt–Ru_{ad}/C)/Nafion™ composite layers containing high metal loadings to Nafion™-117 membranes by hot pressing.

Fig. 5 shows the cell polarization curves measured at 60 and 90 °C. The Pt–Ru_{ad}/C-0.74 (after two depositions) catalyst has the same performance as Pt–Ru_{ad}/C-0.85 (after three deposition cycles), and it is slightly better than Pt–Ru_{ad}/C-0.58 (after a single deposition). This trend is sim-

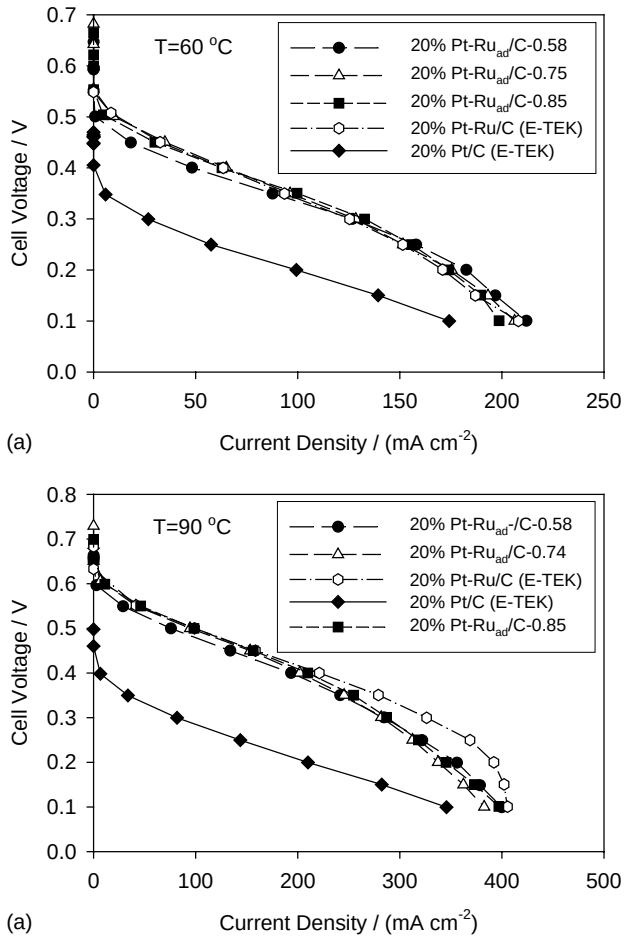

Fig. 5. Polarization curves for DMFCs with carbon-supported Pt–Ru_{ad} anode catalysts. Anode: 0.65 ± 0.2 mg/cm^2 PtRu_{ad}/C (20 wt.% Pt) catalyst, 1.0 M methanol at 4.0 mL/min. Cathode: 2 mg/cm^2 Pt-black catalyst, 20 psig dry oxygen at 400 sccm. Currents are normalized to the geometrical area of the electrodes.

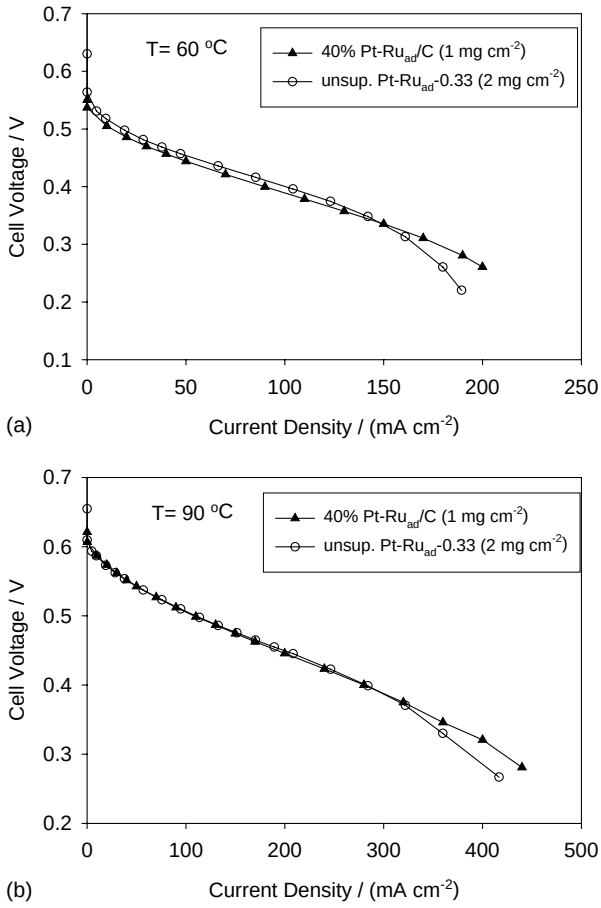

Fig. 6. Comparison of carbon-supported and -unsupported Pt–Ru_{ad} as anode catalyst in a PEM–DMFC. Anode: 1.0 M methanol at 4.0 mL/min. Cathode: 2 mg/cm^2 Pt-black catalyst, 20 psig dry oxygen at 400 sccm. Currents are normalized to the geometrical area of the electrodes.

ilar to that observed for unsupported Pt–Ru_{ad}. The performance of commercially obtained carbon-supported Pt–Ru alloy nanoparticles (E-TEK, 20 wt.% Pt–Ru on Vulcan^{TM} XC-72R, specific surface area: ca. 112 m^2/g) were also determined in these PEM–DMFCs, and the result is included in Fig. 5. The Pt–Ru_{ad}/C was as active as the commercially available Pt–Ru/C at all temperatures studied. Note that the specific surface area of Pt–Ru_{ad}/C and E-TEK Pt–Ru/C are similar. These results show that the supported Pt–Ru_{ad} systems have performances similar to supported Pt–Ru alloy systems in PEM–DMFCs.

A 40 wt.% metal loading Pt–Ru_{ad}/C catalyst was prepared by the surface reductive deposition method using 40 wt.% Pt/C (E-TEK) as the substrate. The relatively high metal content in this 40 wt.% Pt–Ru_{ad}/C catalyst allows the fabrication of an MEA with relatively high anode catalyst loading without a significant increase in the thickness of the catalyst layer. An MEA with anode metal loading of 1 mg/cm^2 was fabricated using this catalyst. Fig. 6 presents the cell polarization curves. Also included in this figure is the performance of an MEA containing 2 mg/cm^2 unsupported Pt–Ru_{ad} anode. It can be seen that the performance of the 1 mg/cm^2 Pt–Ru_{ad}/C (after two depositions) anode is equal to the performance of the 2 mg/cm^2 unsupported Pt–Ru_{ad} catalyst (after two depositions).

3.3. Stability of Pt–Ru_{ad} anode catalysts

Due to the lack of direct techniques to characterize the distribution of Ru_{ad} on highly dispersed nanoparticle Pt–Ru_{ad} surfaces, we used cyclic voltammetry and fuel cell performance to obtain information about possible surface changes of the Pt–Ru_{ad} catalysts. We previously reported the cyclic voltammograms of the various freshly prepared Pt–Ru_{ad} catalysts measured in 1.0 M H_2SO_4 at ambient temperature [Fig. 1 in Ref. [61]]. In this study, we measured the cyclic voltammograms of these Pt–Ru_{ad} nanoparticles after they were incorporated into the anode layer of MEAs, the MEA–DMFCs were conditioned, and then operated for several days. The measurements were carried out in the fuel cell test block at room temperature. The anode served as the working electrode under circulated Ar-purged, purified water. The Pt black cathode was used as counter- and reference electrodes by supplying it with humidified H_2 (1 atm) [67–69]. The potentials are reported versus this reference electrode. Typical CVs are shown in Fig. 7. Currents are normalized to per gram catalysts. It can be seen that, with increasing Ru coverage, the peak resolution in the "hydrogen region" decreases, and currents in the "double-layer region" increase. A sharp peak at ca. 120 mV appears when the Ru coverages are higher than 0.33, and its intensity

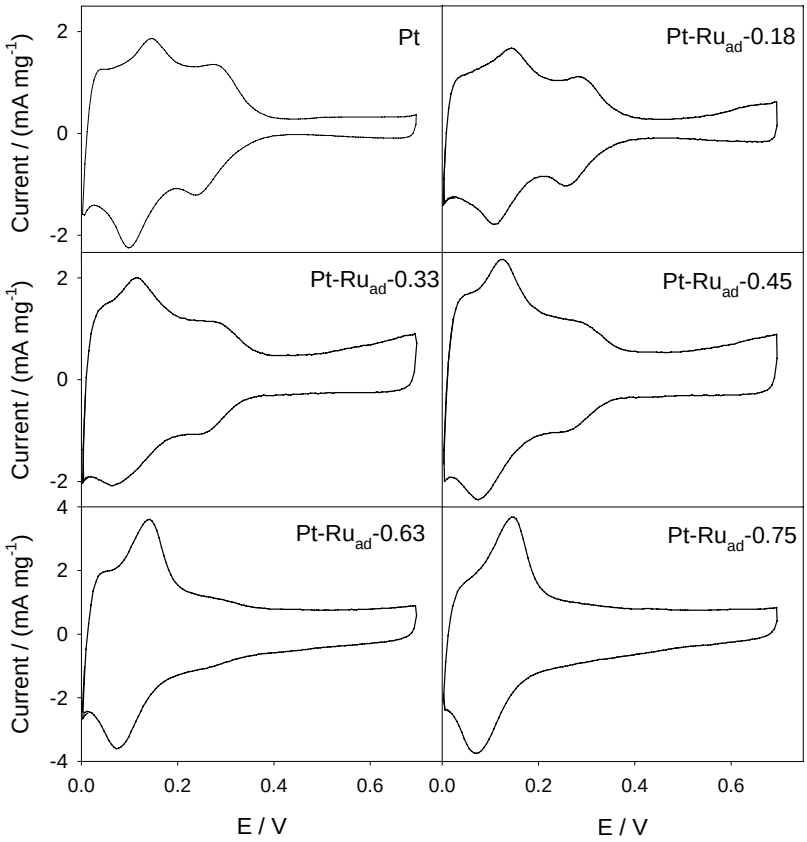

Fig. 7. Cyclic voltammograms of anode catalysts recorded in PEM–DMFCs at 25 °C, 10 mV/s sweep rate. The anode catalyst loading is 2 mg/cm^2.

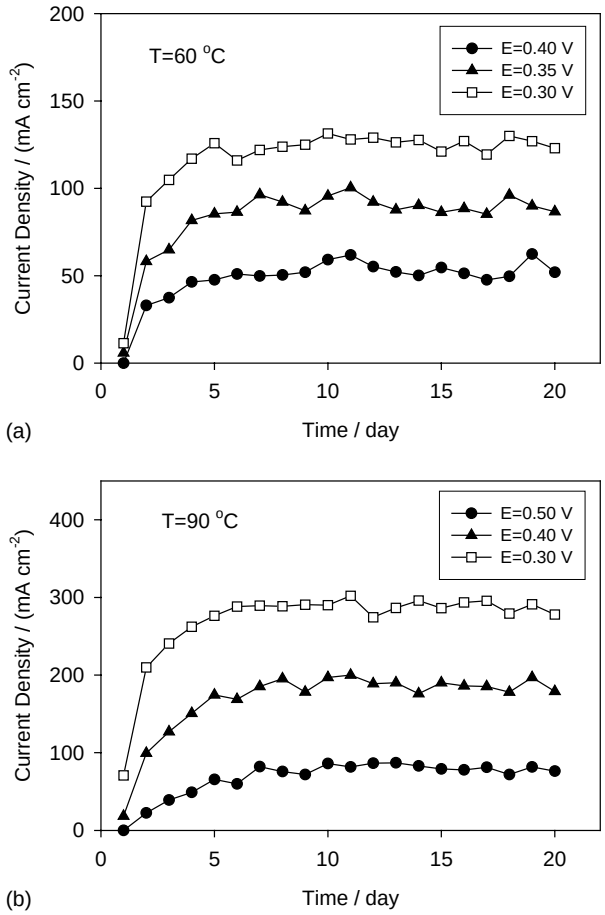

Fig. 8. Durability test for the PEM–DMFC with Pt–Ru_{ad}/C anode catalyst. Anode: 0.68 mg/cm^2 Pt–Ru_{ad}/C-0.58 (20 wt.% Pt) catalyst, 1.0 M methanol at 4.0 mL/min. Cathode: 2 mg/cm^2 Pt-black catalyst, 20 psig dry oxygen at 400 sccm. Currents are normalized to the geometrical area of the electrode.

increases with Ru coverage. All these features closely resemble those we previously observed on freshly prepared Pt–Ru_{ad} in H_2SO_4. [Fig. 1 in Ref. [61]] Comparison of the individual CVs recorded in MEA to those recorded in H_2SO_4 for the same Pt–Ru_{ad} shows that no significant changes occur before and after hot-pressing into an MEA and operation of the DMFC. Cyclic voltammetry, therefore, indicates that no significant surface reconstructions (Ru redistribution and dissolution) were observed for Pt–Ru_{ad} during the fabrication of the MEAs.

The moderate-term stability of the PEM–DMFC with Pt–Ru_{ad}/C-0.58 (20 wt.% Pt) anode catalyst was tested at 60 and 90 °C. These data are shown in Fig. 8. The cell was run for a total of 20 days at 8 h per day. A typical day operation procedure is as follows. First, the cell was heated to 60 °C at open circuit (ca. 10 min) with 1.0 M aqueous methanol circulating through the anode compartment, and oxygen flowing through the cathode at 20 psig back pressure. The cell was then operated at 20 mA/cm^2 (ca. 0.45 V) for 1.5 h, at 50 mA/cm^2 (ca. 0.4 V) for 1 h, and at 100 mA/cm^2 (ca. 0.35 V) for another hour. The cell was then polarized by sweeping the cell potential back and forth from open circuit to 0.1 V several times until a reproducible polarization curve was obtained (ca. 10 cycles). After the sweeps, the cell current was held at 100 mA/cm^2, and the cell was heated to 90 °C (ca. 10 min). The cell was then operated at 100 mA/cm^2 (ca. 0.45 V) for 1.5 h, and 200 mA/cm^2 (ca. 0.35 V) for another 1.5 h. Potential sweeps were performed again. Finally, the electronic load and heating were turned off, and the methanol and oxygen supply were shut down. As shown in Fig. 8, no loss in performance was observed over 20 days operation. This result indicates that no Ru dissolution and/or redistribution occurred that is large enough to affect the catalytic activity.

4. Conclusions

Unsupported and carbon supported nanoparticle Pt–Ru_{ad} catalysts prepared using the surface reductive deposition technique were evaluated as anode catalysts in liquid feed PEM–DMFCs. It was found that the surface composition of unsupported Pt–Ru_{ad} nanoparticles has a significant influence on their activities as anode catalysts in DMFCs. The optimum Ru surface coverage was ca. 33% for DMFCs operating at 60 °C, and ca. 30–60% for DMFCs operating at 90 °C. Carbon-supported Pt–Ru_{ad} catalysts display higher mass activities than unsupported Pt–Ru_{ad}. Comparable cell performance can be obtained using carbon-supported Pt–Ru_{ad} with much lower metal loading than unsupported. The maximum power density measured on Pt–Ru_{ad} approaches 70% of that obtained on the state-of-the-art commercial Pt–Ru alloy catalyst from Johnson Matthey, despite the specific surface area of Pt–Ru_{ad} being only 40% that of the Johnson Matthey Pt–Ru catalyst. Cyclic voltammetry showed that no obvious surface restructuring of Pt–Ru_{ad} occurred during the fabrication and operation of the DMFCs. A PEM–DMFC using Pt–Ru_{ad}/C anode catalyst was operated for 20 days on an intermittent basis with no obvious deterioration in the cell performance. This result shows that Pt–Ru_{ad} nanoparticle catalysts should be explored further as catalysts in practical DMFCs.

Acknowledgements

We thank Dr. Youbin Shao and Professor Gary Horlick at the University of Alberta for their kind, expert assistance with inductively coupled plasma spectrophotometry measurements. We thank the Natural Sciences and Engineering Research Council of Canada and the University of Alberta for supporting this work.

References

[1] S. Wasmus, A. Kuver, J. Eectroanal. Chem. 461 (1999) 14.
[2] M. Watanabe, S. Motoo, J. Electroanal. Chem. 60 (1975) 267.

[3] K.L. Ley, R. Liu, C. Pu, Q. Fan, N. Leyarovska, C. Segre, E.S. Smotkin, J. Electrochem. Soc. 144 (1997) 1543.
[4] E. Reddington, A. Sapienza, B. Gurau, R. Viswanathan, S. Sarangapani, E.S. Smotkin, T.E. Mallouk, Science 280 (1998) 1735.
[5] A.N. Frumkin, B.I. Podlovchenko, Ber. Akad. Wiss. USSR 150 (1963) 34.
[6] J.O'M. Bockris, H. Wroblowa, J. Electroanal. Chem. 7 (1964) 428.
[7] O.A. Petry, B.I. Podlovchenko, A.N. Frumkin, H. Lal, J. Eectroanal. Chem. 10 (1965) 253.
[8] X.M. Ren, P. Zelenay, S. Thomas, J. Davey, S. Gottesfeld, J. Power Sources 86 (2000) 111.
[9] B.D. McNicol, D.A.J. Rand, K.R. Williams, J. Power Sources 83 (1999) 15.
[10] E. Herrero, K. Franaszczuk, A. Wieckowski, J. Electroanal. Chem. 361 (1993) 269.
[11] W. Chrzanowski, A. Wieckowski, Langmuir 14 (1998) 1967.
[12] G. Tremiliosi-Filho, H. Kim, W. Chrzanowski, A. Wieckowski, B. Grzybowska, P. Kulesza, J. Electroanal. Chem. 467 (1999) 143.
[13] W.F. Lin, M.S. Zei, M. Eiswirth, G. Ertl, T. Iwasita, W. Vielstich, J. Phys. Chem. B 103 (1999) 6968.
[14] S. Cramm, K.A. Friedrich, K.-P. Geyzers, U. Stimming, R. Vogel, Fresen. J. Anal. Chem. 358 (1997) 189.
[15] K.A. Friedrich, K.-P. Geyzers, A. Marmann, U. Stimming, R. Vogel, Z. Phys. Chem. 208 (1999) 137.
[16] K.A. Friedrich, K.-P. Geyzers, U. Linke, U. Stimming, J. Stumper, J. Electroanal. Chem. 402 (1996) 123.
[17] K.A. Friedrich, K.-P. Geyzers, A.J. Dickinson, U. Stimming, J. Electroanal. Chem. 524 (2002) 261.
[18] G. Samjeske, X.Y. Xiao, H. Baltruschat, Langmuir 18 (2002) 4659.
[19] M. Watanabe, Y. Genjima, K. Turumi, J. Electrochem. Soc. 144 (1997) 423.
[20] F. Vigier, F. Gloaguen, J.M. Leger, C. Lamy, Electrochim. Acta 46 (2001) 4331.
[21] T. Frelink, W. Visscher, J.A.R. van Veen, Surf. Sci. 335 (1995) 353.
[22] T. Frelink, W. Visscher, J.A.R. van Veen, Langmuir 12 (1996) 3702.
[23] T.D. Jarvi, T.H. Madden, E.M. Stuve, Electrochem. Solid State Lett. 2 (1999) 224.
[24] T. Iwasita, H. Hoster, A. John-Anacker, W.F. Lin, W. Vielstich, Langmuir 16 (2000) 522.
[25] H. Hoster, T. Iwasita, H. Baumgartner, W. Vielstich, Phys. Chem. Chem. Phys. 3 (2001) 337.
[26] J.C. Davies, B.E. Hayden, D.J. Pegg, Electrochim. Acta 44 (1998) 1181.
[27] J.C. Davies, B.E. Hayden, D.J. Pegg, Surf. Sci. 467 (2000) 118.
[28] J.C. Davies, B.E. Hayden, D.J. Pegg, M.E. Rendall, Surf. Sci. 496 (2002) 110.
[29] C. Lu, C. Rice, R.I. Masel, P.K. Babu, P. Waszczuk, H.S. Kim, E. Oldfield, A. Wieckowski, J. Phys. Chem. B 106 (2002) 9581.
[30] P. Waszczuk, G.Q. Lu, A. Wieckowski, C. Lu, C. Rice, R.I. Masel, Electrochim. Acta 47 (2002) 3637.
[31] W. Chrzanowski, A. Wieckowski, Langmuir 13 (1997) 5974.
[32] W. Chrzanowski, H. Kim, A. Wieckowski, Catal. Lett. 50 (1998) 69.
[33] H. Kim, I.R. de Moraes, G. Tremiliosi-Filho, R. Haasch, A. Wieckowski, Surf. Sci. 474 (2001) L203.
[34] A. Crown, H. Kim, G.Q. Lu, I.R. de Moraes, C. Rice, A. Wieckowski, J. New Mat. Elect. Syst. 3 (2000) 275.
[35] P. Waszczuk, J. Solla-Gullon, H.S. Kim, Y.Y. Tong, V. Montiel, A. Aldaz, A. Wieckowski, J. Catal. 203 (2001) 1.
[36] Y.Y. Tong, H.S. Kim, P.K. Babu, P. Waszczuk, A. Wieckowski, E. Oldfield, J. Am. Chem. Soc. 124 (2002) 468.
[37] A. Crown, A. Wieckowski, Phys. Chem. Chem. Phys. 3 (2001) 3290.
[38] C. Rice, S. Ha, R.I. Masel, A. Wieckowski, J. Power Sources 115 (2003) 229.
[39] E. Herrero, J.M. Feliu, A. Wieckowski, Langmuir 15 (1999) 4944.
[40] A. Crown, C. Johnston, A. Wieckowski, Surf. Sci. 506 (2002) L268.
[41] A. Crown, I.R. Moraes, A. Wieckowski, J. Electroanal. Chem. 500 (2001) 333.
[42] Y.Y. Tong, A. Wieckowski, E. Oldfield, J. Phys. Chem. B 106 (2002) 2434.
[43] C.E. Lee, P.B. Tiege, Y. Xing, J. Nagendran, S.H. Bergens, J. Am. Chem. Soc. 119 (1997) 3543.
[44] C.E. Lee, S.H. Bergens, J. Phys. Chem. B 102 (1998) 193.
[45] D.X. Cao, S.H. Bergens, J. Electroanal. Chem. 533 (2002) 91.
[46] E.R. Fachini, C.R. Cabrera, Langmuir 15 (1999) 717.
[47] E.R. Fachini, R. Diaz-Ayala, E. Casado-Rivera, S. File, C.R. Cabrera, Langmuir 19 (2003) 8986.
[48] M.M.P. Janssen, J. Moolhuysen, Electrochim. Acta 21 (1976) 861.
[49] M.M.P. Janssen, J. Moolhuysen, Electrochim. Acta 21 (1976) 869.
[50] S. Szabó, I. Bakos, J. Electroanal. Chem. 230 (1987) 233.
[51] S. Szabó, I. Bakos, F. Nagy, J. Electroanal. Chem. 271 (1989) 269.
[52] P. Del Angel, J.M. Dominguez, G. Del Angel, J.A. Montoya, J. Capilla, E. Lamy-Pitara, J. Barbier, Top. Catal. 18 (2002) 183.
[53] P. Del Angel, J.M. Dominguez, G. Del Angel, J.A. Montoya, E. Lamy-Pitara, S. Labruquere, J. Barbier, Langmuir 16 (2000) 7210.
[54] J.M. Dumas, S. Rmili, J. Barbier, J. Chim. Phys. PCB 95 (1998) 1650.
[55] C. Micheaud-Especel, D. Bazin, M. Guerin, P. Marecot, J. Barbier, React. Kinet. Catal. Lett. 69 (2000) 209.
[56] C. Micheaud, P. Marecot, M. Guerin, J. Barbier, Appl. Catal. A-Gen. 171 (1998) 229.
[57] C.L. Pieck, P. Marecot, J. Barbier, Appl. Catal. A-Gen. 134 (1996) 319.
[58] C.L. Pieck, P. Marecot, J. Barbier, Appl. Catal. A-Gen. 141 (1996) 229.
[59] C.L. Pieck, P. Marecot, J. Barbier, Appl. Catal. A-Gen. 143 (1996) 283.
[60] J.M. Dumas, C. Geron, H. Hadrane, P. Marecot, J. Barbier, J. Mol. Catal. 77 (1992) 87.
[61] D.X. Cao, S.H. Bergens, Electrochim. Acta 48 (2003) 4021.
[62] H.A. Gasteiger, P.N. Ross, E.J. Cairns, Surf. Sci. 293 (1993) 67.
[63] N.M. Markovic, P.N. Ross, Surf. Sci. Rep. 45 (2002) 121.
[64] A.S. Arico, P.L. Antonucci, E. Modica, V. Baglio, H. Kim, V. Antonucci, Electrochim. Acta 47 (2002) 3723.
[65] A. van der Wiel, Chem. Weekblad. 48 (1952) 597.
[66] R. Woods, J. Electroanal. Chem. 49 (1974) 217.
[67] S.C. Thomas, X.M. Ren, S. Gottesfeld, J. Electrochem. Soc. 146 (1999) 4354.
[68] H.N. Dinh, X.M. Ren, F.H. Garzon, P. Zelenay, S. Gottesfeld, J. Electroanal. Chem. 491 (2000) 222.
[69] C.Z. He, Z.Q. Qi, M. Hollett, A. Kaufman, Electrochem. Solid-State Lett. 5 (2002) A181.
[70] H.A. Gasteiger, N. Markovic, P.N. Ross, E.J. Cairns, J. Electrochem. Soc. 141 (1994) 1795.
[71] M. Neergat, D. Leveratto, U. Stimming, Fuel Cells 2 (2002) 25.
[72] C. Coutanceau, A.F. Rakotondrainibe, A. Lima, E. Garnier, S. Pronier, J.M. Leger, C. Lamy, J. Appl. Electrochem. 34 (2004) 61.
[73] L. Dubau, C. Coutanceau, E. Garnier, J.M. Leger, C. Lamy, J. Appl. Electrochem. 33 (2003) 419.
[74] D.X. Cao, Doctorate Thesis, Spring, 2004.
[75] C.L. Green, A. Kucernak, J. Phys. Chem. B 106 (2002) 1036.
[76] S. Gottesfeld, T. Zawodzinski, Polymer electrolyte fuel cells, in: C. Tobias, H. Gerischer, D. Kolb, R. Alkire (Eds.), Advances in Electrochemistry and Electrochemical Engineering, vol. 5, Wiley/VCH, New York, 1997, p. 195.
[77] V. Metha, J.S. Cooper, J. Power Source 114 (2003) 32.
[78] A.S. Arico, P. Creti, Z. Poltarzewski, R. Mantegna, H. Kim, N. Giordano, V. Antonucci, Mater. Chem. Phys. 47 (1997) 257.
[79] A.S. Arico, P. Creti, N. Giordano, V. Antonucci, P.L. Antonucci, A. Chuvilin, J. Appl. Electrochem. 26 (1996) 959.
[80] P. Argyropoulos, K. Scott, W.M. Taama, Electrochim. Acta 44 (1999) 3575.

[81] P. Argyropoulos, K. Scott, W.M. Taama, J. Appl. Electrochem. 29 (1999) 661.
[82] K. Scott, W.M. Taama, P. Argyropoulos, K. Sundmacher, J. Power Sources 83 (1999) 204.
[83] W.E. O'Grady, P.L. Hagans, K.I. Pandya, D.L. Maricle, Langmuir 17 (2001) 3047.
[84] X.M. Ren, M.S. Wilson, S. Gottesfeld, J. Electrochem. Soc. 143 (1996) L12.
[85] K. Scott, P. Argyropoulos, P. Yiannopoulos, W.M. Taama, J. Appl. Electrochem. 31 (2001) 823.
[86] K. Scott, W.M. Taama, P. Argyropoulos, J. Power Sources 79 (1999) 43.
[87] J.C. Amphlett, B.A. Peppley, E. Halliop, A. Sadiq, J. Power Sources 96 (2001) 204.
[88] L. Liu, G. Pu, R. Viswanathan, Q.B. Fan, R.X. Liu, E.S. Smotkin, Electrochim. Acta 43 (1998) 3657.